INORGANIC CHEMISTRY FRONTIERS

RESEARCH ARTICLE

View Article Online
View Journal | View Issue

Cite this: *Inorg. Chem. Front.*, 2024, **11**, 8130

Equivalent cation-tuning to realize a new Ce(IV) fluoride with excellent comprehensive nonlinear optical performances†

Bei-Bei Zhang,‡ Wen-Ye Gao,‡ Wei Xu, Liang Ma, Wenlong Liu, Ru-Ling Tang * and Sheng-Ping Guo

Received 16th August 2024,
Accepted 27th September 2024

DOI: 10.1039/d4qi02088j

rsc.li/frontiers-inorganic

Exploring nonlinear optical (NLO) halide materials has become a hot research field owing to their diverse structures and excellent optical properties. In this paper, a new inorganic tetravalent cerium fluoride $NH_4Ce_3F_{13}$ was obtained. It crystallizes in the polar space group of $Pmc2_1$ and exhibits a three-dimensional $\{[Ce_3F_{13}]^-\}_\infty$ framework, which is composed of $\{[CeF_8]^{4-}\}_\infty$ chains and $\{[CeF_6]^{2-}\}_\infty$ layers formed by CeF_9 polyhedra, with the NH_4^+ cation balancing the charge. $NH_4Ce_3F_{13}$ exhibits a strong second-harmonic generation (SHG) response among inorganic metal fluorides of about 1.2 times greater than that of KH_2PO_4 (KDP) and a high laser-induced damage threshold (LIDT), which is 39 times more than that of $AgGaS_2$. Besides, $NH_4Ce_3F_{13}$ possesses the largest band gap among Ce(IV)-containing NLO materials. This work provides a good case for exploring high-performance NLO fluoride materials.

Introduction

Metal halides play an important role in the field of photoelectronic functional materials. They are widely used in photovoltaics, light-emitting diodes (LEDs), nonlinear optical (NLO) materials, and laser technology on account of their diverse structural features and excellent photoelectric properties.[1–4] In the past several years, several NLO metal halides, including $K_2SbF_2Cl_3$, $Pb_7F_{12}Cl_2$, $BaClBF_4$, Ag_2HgI_4, $HgBr_2$, $CsHgBr_3$, $Cs_2HgI_2Cl_2$, $Rb_2CdBr_2I_2$, Rb_2CdBrI_3, and $Rb_4Sn_3Cl_2Br_8$, have been reported. Some of them exhibit strong SHG effects and high laser-induced damage thresholds (LIDTs), such as $Pb_7F_{12}Cl_2$, $HgBr_2$, and Rb_2CdBrI_3.[5–14] In addition, some metal halides with stereochemically active lone-pair electrons (LPEs) exhibit excellent optical anisotropy. For example, A_3SnCl_5, ASn_2Cl_5 (A = NH_4 and Rb), $A_2Sn_2F_5Cl$, and $ASnFCl_2$ (A = Rb and Cs) exhibit outstanding birefringence and a wide transparent region.[15,16]

In recent years, NLO metal fluoride crystals have attracted more attention. The combination of the strongest electronegative F atom and metal cations can form compounds with excellent optical performances. Many NLO fluorides have been investigated, such as SbF_3, $NaSb_3F_{10}$, $BaZnF_4$, KBi_4F_{13}, $SrAlF_5$, KNa_2ZrF_7, $K_3Ba_2Zr_6F_{31}$, $K_2BaM_2F_{12}$, and Li_2CaMF_8 (M = Zr and Hf).[17–25] Evidently, Zr- and Hf-based fluorides show large optical band gaps and high LIDTs, such as KNa_2ZrF_7. Attractively, $K_3Ba_2Zr_6F_{31}$, $K_2BaM_2F_{12}$ and Li_2CaMF_8 (M = Zr and Hf) possess a wide transparency window below 200 nm. However, although fluorides have advantages in generating compounds with large band gaps, most acentric fluoride crystals show weaker SHG intensity than commercial NLO crystal KH_2PO_4 (KDP). Apart from group IVB metal fluorides, our group studied cerium(IV) fluorides owing to their similar ionic radii and valence states. Based on these studies, highly electropositive cations (Zr^{4+}, Ti^{4+}, Hf^{4+}, Ce^{4+}, *etc.*) could lead to diverse asymmetric structural units and thus produce many interesting crystal structures and promising NLO properties. To date, except for lone pair electronic metal fluorides, only Na_2CeF_6 exhibits an SHG intensity stronger than KDP (2.1 × KDP).[26] Clearly, tetravalent cerium fluorides have great potential for NLO performance. To date, among Ce(IV)-containing fluorides, only Na_2CeF_6 has been reported to show SHG effects. Hence, exploring new fluorides containing Ce(IV) is a meaningful task not just for exploring new NLO materials, but also for enriching the structural diversity of rare earth fluorides. Designing new acentric fluorides is the prerequisite for obtaining new NLO Ce(IV) fluoride materials. In current popular design strategies, the synthesis of new NLO materials using isovalent ion substitution based on non-centrosymmetric (NCS) or centrosymmetric (CS) parent compounds is an effective approach. Generally, different ionic radii may cause structural changes and variations in SHG activity. In recent years, several new NLO compounds have been discov-

School of Chemistry and Chemical Engineering, Yangzhou University, Yangzhou, Jiangsu 225002, P. R. China. E-mail: rltang@yzu.edu.cn

†Electronic supplementary information (ESI) available: Additional tables and figures. CCDC 2371443. For ESI and crystallographic data in CIF or other electronic format see DOI: https://doi.org/10.1039/d4qi02088j

‡These authors contributed equally to this work.

ered through equivalent ion regulation strategies. For instance, the NCS compounds $CsNaTaF_7$ were obtained from CS compound $CsKTaF_7$ by substituting the alkali–metal cation. CS-to-NCS structural transformation can be achieved from $Cs_2M_3(P_2O_7)_2$ (M = Zn and Mg) to $Rb_2Zn_3(P_2O_7)_2$, as well as from $K_2YB_3O_6F_2$ to $A_2YB_3O_6F_2$ (A = Cs, Rb), achieving CS to NCS structural transformation. The substitution of Li^+ to K^+ results in optimizing the optical properties of α-$AZnPO_4$ (A = Li, K). The physical properties vary due to the different cations based on the AB_4O_6F (A = NH_4, Na, K, Rb, and Cs) family. The NLO carbonates $ABCO_3F$ (A = K, Rb, Cs; B = Ca, Sr, Ba) were designed by adjusting the metal cations. A series of NLO rare-earth borates, $K_7MRE_2B_{15}O_{30}$ (M = Zn, Cd, Pb; RE = Sc, Y, Gd, Lu), were also obtained by the substitution of isovalent cations.[27–38] Obviously, isovalent cation regulation is a preferred method for developing new NLO materials.

According to the above thoughts, a new ammonium cerium(IV) fluoride crystal, $NH_4Ce_3F_{13}$, was obtained by a hydrothermal reaction. It adopts the acentric space group of $Pmc2_1$ and shows a phase-matching SHG effect. Synthesis, crystal structure, and the relationship between structure and performance based on theoretical calculations are presented in this work.

Experimental section

Synthesis

All commercial reagents of CeO_2 (Tansoole, 99.99%), NH_4F (Sinopharm, AR), ZnF_2 (Sinopharm, AR), and HF solution (40% in water, by weight) were used as received. Caution! Hydrofluoric acid is toxic and volatile. Proper precautions and extreme caution must be exercised during the experiment. The single crystals of $NH_4Ce_3F_{13}$ were obtained by applying the hydrothermal method. A mixture of NH_4F (0.9 mmol), CeO_2 (1.8 mmol), and ZnF_2 (0.3 mmol) was put into the 23 mL Teflon liners with adding 1.5 mL of HF and 3 mL of deionized water solution. Then, the sealed Teflon liners in the oven were heated to 230 °C for 1 day and cooled to room temperature for 2 days. Finally, colourless single crystals (inset of Fig. 3) of $NH_4Ce_3F_{13}$ were obtained with yields of 28–35% based on CeO_2.

Single crystal structure determination

The crystal data of $NH_4Ce_3F_{13}$ were collected by applying a Bruker D8 QUEST X-ray diffractometer with graphite-monochromated Mo-Kα radiation (λ = 0.71073 Å). The structures were solved using direct methods refined by full-matrix least-squares techniques on F^2 with anisotropic displacement parameters for all atoms. The PLATON program was used to check the correctness of the structure, and no errors were found.[39,40] The crystallographic data and refinement parameters of $NH_4Ce_3F_{13}$ are shown in Table 1. Bond lengths, bond angles, atomic coordinates and equivalent isotropic displacement parameters are summarized in Tables S1–S4,† respectively. CCDC number 2371443† was assigned to the deposition of $NH_4Ce_3F_{13}$.

Table 1 Crystal data and structure refinement parameters for $NH_4Ce_3F_{13}$

Empirical formula	$NH_4Ce_3F_{13}$
Mr (g mol^{-1})	685.40
Cryst syst.	Orthorhombic
T (K)	296(2)
Space group	$Pmc2_1$
a (Å)	7.9167(8)
b (Å)	7.2697(7)
c (Å)	8.3413(7)
V (Å^3)	480.06(8)
Z	2
D_c (g cm^{-3})	4.742
μ(mm^{-1})	14.161
F(000)	604.0
Crystal size/mm^3	0.12 × 0.11 × 0.1
Radiation	MoKα (λ = 0.71073)
2θ range for data collection/°	5.146 to 54.952
Index ranges	$-6 \le h \le 10$, $-9 \le k \le 9$, $-10 \le l \le 9$
Reflns collected	2327
Independent reflections	1046 [R_{int} = 0.0287, R_{sigma} = 0.0393]
Data/restraints/parameters	1046/10/99
Goodness-of-fit on F^2	1.047
Final R indexes [$I \ge 2\sigma(I)$]^{a,b}	R_1 = 0.0178, wR_2 = 0.0380
Final R indexes [all data]^{a,b}	R_1 = 0.0182, wR_2 = 0.0382
Largest diff. peak/hole/e Å^{-3}	0.76/−1.35
Flack parameter	0.030(19)

^{a} $R_1 = ||F_o| - |F_c||/|F_o|$. ^{b} w$R_2 = [w(F_o^2 - F_c^2)^2]/[w(F_o^2)^2]]^{1/2}$.

Energy-dispersive X-ray spectroscopy (EDS)

EDS analysis of selected several crystals was performed using a Bruker quantum dispersive X-ray spectroscope, which confirms the presence of N, Ce and F in the crystals. The EDS elemental analysis images for the single crystals and the molar ratios of N/Ce/F are shown in Fig. S2 and Table S5,† respectively.

Powder X-ray diffraction (PXRD) analysis

The PXRD characterization for the $NH_4Ce_3F_{13}$ sample was collected using a Smart Lab powder X-ray diffractometer for Cu Kα radiation (λ = 1.5406 Å), with the 2θ range of 10–70° and a scan speed of 0.1 s per step. The simulated patterns were generated on the Mercury v3.8 program using the single-crystal structure data of $NH_4Ce_3F_{13}$. The experimental and simulated PXRD patterns match well, suggesting that the obtained sample is pure (Fig. 1).

Thermogravimetric analysis

Thermogravimetric characterization was performed on Netzsch STA 449 F3 in flowing N_2 gas. The powder sample was placed in an alumina crucible with a heating procedure ranging from 20 to 1000 °C at a rate of 15 °C per minute.

Optical properties

The IR spectrum was measured using a Magna 750 FI-IR spectrometer with a wavelength of 4000–400 cm^{-1} with pure KBr as the background. The pure $BaSO_4$ sample was used as the standard reference. The UV–vis–NIR diffuse reflectance spectrum of $NH_4Ce_3F_{13}$ was collected using a Carry 5000 spectrometer in the range of 200–800 nm. The reflection spectrum was calculated using the Kubelka–Munk function to calculate the band gap.

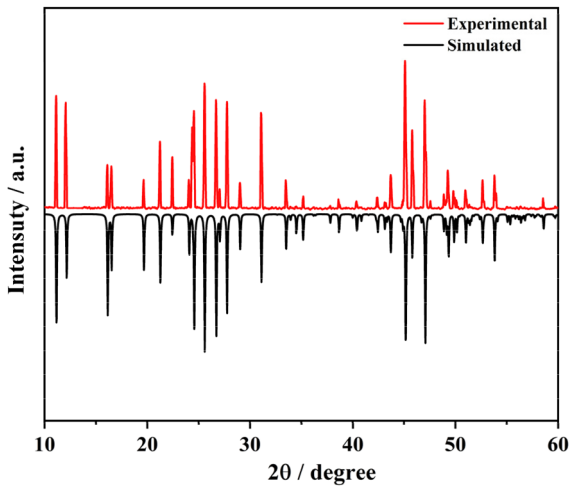

Fig. 1 Simulated and experimental powder X-ray diffraction patterns of $NH_4Ce_3F_{13}$.

Second-harmonic generation and laser-induced damage threshold (LIDT) measurements

The SHG response of the $NH_4Ce_3F_{13}$ powder sample was measured by applying the Kurtz and Perry method using a Q-switched Nd:YAG laser under 1064 nm. The frequency-doubling effect depended largely on the granular size, so the sample was sieved into six consecutive sizes (25–45, 45–75, 75–105, 105–150, 150–200 and 200–250 μm), with KDP samples of the same size used as the reference. The single-pulse measurement method was used to measure the LIDTs of $NH_4Ce_3F_{13}$, with $AgGaS_2$ (AGS) selected for comparison under the same conditions. The samples were radiated with a 1064 nm laser with a pulse width τ_p of 10 ns in a 1 Hz repetition. The laser emission energy was adjusted by a Nova II sensor display with a PE50-DIT-C energy sensor until the damaged spot was observed.

Theoretical calculation

The theoretical calculations of electronic structure, optical properties and the density of states (DOS) were carried out on the CASTEP mode based on the density functional theory (DFT) method. The generalized gradient approximation (GGA) and the Perdew–Burke–Ernzerhof (PBE) function were applied for the exchange–correlation energy.[41–43] The orbital electrons of each atom as valence electrons were H $1s^1$, N $2s^22p^3$, F $2s^22p^5$ and Ce $4f^15d^16s^2$. The cut-off kinetic energy of 410 eV was adopted, and the Brillouin zone numerical integration was implemented by employing 4 × 3 × 3 for Monkhorst–Pack *k*-point sampling to determine the numbers of plane waves, with the Fermi level setting at zero as the energy reference.

Results and discussion

Crystal structure

$NH_4Ce_3F_{13}$ crystallizes in the orthorhombic space group $Pmc2_1$, which includes two kinds of Ce, one unique N, and nine types of F atoms in the asymmetric unit. The crystal structure of $NH_4Ce_3F_{13}$ consists of NH_4^+ cations and the 3D $\{[Ce_3F_{13}]^-\}_\infty$ anion framework. Both Ce(1) and Ce(2) atoms are connected with nine F atoms to construct the CeF_9 polyhedra (Fig. S1†). The Ce(1)F_9 polyhedra are linked together *via* corner-sharing F(2) atoms along the *c* axis to form $\{[Ce(1)F_8]^{4-}\}_\infty$ chains (Fig. 2a), whereas the Ce(2)F_9 polyhedra are bonded together *via* edge-sharing to make up $\{[Ce(2)F_6]^{2-}\}_\infty$ layers in the *ac* plane (Fig. 2b). Furthermore, the $\{[Ce(1)F_8]^{4-}\}_\infty$ chains are corner- and edge-shared with $\{[Ce(2)F_6]^{2-}\}_\infty$ layers to construct the 3D $\{[Ce_3F_{13}]^-\}_\infty$ framework, with NH_4^+ distributed in the cavity to balance the charge (Fig. 2c). The Ce–F and N–H bond distances are in the ranges of 2.197(6)–2.455(4) Å and 0.847(7)–0.851(1) Å, respectively.

The reported inorganic monovalent cation Ce(IV)-based fluorides are summarized in Table S6† for comparison with $NH_4Ce_3F_{13}$. In Na_2CeF_6 ($P\bar{6}2m$) and $LiCeF_5$ ($I4_1/a$), Ce atoms also form CeF_9 polyhedra.[26,44] Cs_3CeF_7 ($Fm\bar{3}m$) and Rb_3CeF_7 ($Fm\bar{3}m$) feature 3D frameworks composed of CeF_6 polyhedra. $CsCeF_5$ ($P2_1/c$), Na_3CeF_7 ($I4/mmm$), Li_4CeF_8 ($Pnma$), $(NH_4)_7Ce_6F_{31}$ ($R\bar{3}$), $(NH_4)_2CeF_6$ ($Pbcn$) and $(NH_4)_4CeF_8$ ($C2/c$) comprised CeF_8 polyhedra to display 3D frameworks.[45–50] In the structure of $LiCeF_5$, the distorted CeF_9 polyhedra form $\{[CeF_6]^{2-}\}_\infty$ chains by edge-sharing along the *c* axis. Then, these chains are linked together *via* corner sharing to build a 3D $\{[CeF_5]^-\}_\infty$ framework. To date, only Na_2CeF_6 has been reported as an NLO material. Although the two compounds are composed of CeF_9 polyhedra, it is noteworthy that the arrangements of CeF_9 polyhedra have transformed. Na_2CeF_6 only contains one Ce atom, which forms $\{[CeF_6]^{2-}\}_\infty$ chains, with the 3D $\{[Na_6F_{18}]^{12-}\}_\infty$ framework to build the whole structure

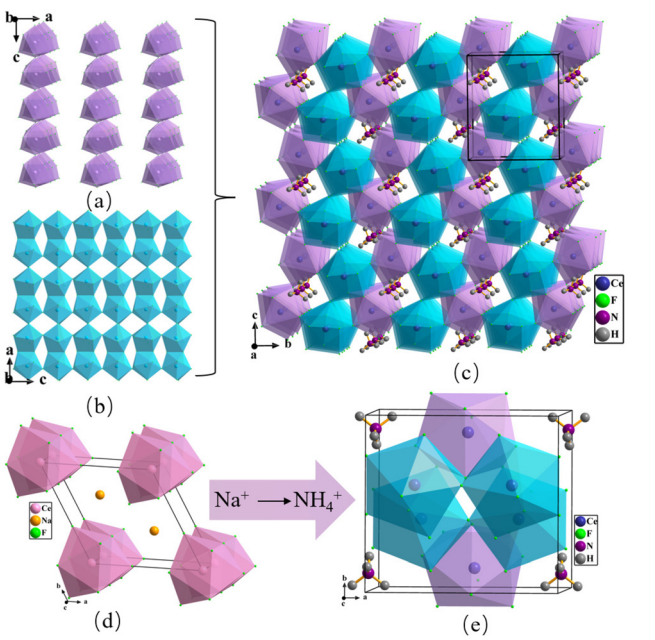

Fig. 2 Crystal structure of $NH_4Ce_3F_{13}$. The arrangements of $\{[Ce(1)F_8]^{4-}\}_\infty$ chains along the *c* axis (a). $\{[CeF_6]^{2-}\}_\infty$ layers in the *ac* plane (b). The whole three-dimensional crystal structure viewed along the *c* direction (c). Unit-cell structures of Na_2CeF_6 (d) and $NH_4Ce_3F_{13}$ (e).

(Fig. S3†). However, there are two kinds of Ce atoms in $NH_4Ce_3F_{13}$, showing two different structural parts, $\{[CeF_8]^{4-}\}_\infty$ chains and $\{[CeF_6]^{2-}\}_\infty$ layers, and then further to build a 3D $\{[Ce_3F_{13}]^-\}_\infty$ framework. Besides, the Na–F bond distances are in the range of 2.2748(11)–2.6453(6) Å, which are close to the bond distances of Ce–F in the range of 2.182(2)–2.370(2) Å, so it can be observed that the structure of Na_2CeF_6 is composed of MF_9 (M = Na, Ce) polyhedra. When the Na^+ cation is substituted by an NH_4^+ cation with a larger ionic radius, NH_4^+ cations are further away from CeF_9 polyhedra, resulting in the CeF_9 polyhedra adopting different configurations to fit different cations, from 1D chains in Na_2CeF_6 to a 3D framework in $NH_4Ce_3F_{13}$, which further leads to structural transformation. On the other hand, fluorides with the same number of fluorine atoms in the formulae are summarized in Table S7,† including KBi_4F_{13} ($I\bar{4}$), $NH_4Sb_4F_{13}$ ($I\bar{4}$), KSb_4F_{13} ($I\bar{4}$), RbU_3F_{13} ($Pmc2_1$), NH_4UF_{13} ($Pmc2_1$), $RbTh_3F_{13}$ ($Pmc2_1$) and $[(C_5H_6N_2)_2H](Sb_4F_{13})$ ($P1$).[20,51–56] RbU_3F_{13}, NH_4UF_{13} and $RbTh_3F_{13}$ are isotypes with the title compound, but these compounds are radioactive and have only been reported on their structures without studying the SHG effects. The structures of the three compounds also feature a combination of layers and chains consisting of edge- and corner-shared MF_9 (M = U and Th) polyhedra.

Optical measurements

The IR spectrum shows two distinct absorption peaks (Fig. 3). The peaks at 3240 and 1417 cm^{-1} are related to the N–H vibrations of NH_4^+, which is close to the reported compounds containing NH_4^+.[57,58] As the UV–vis–NIR diffuse reflectance spectrum shown in Fig. 4, the optical band gap of $NH_4Ce_3F_{13}$ is determined to be 4.26 eV, which is the largest among Ce(IV)-containing NLO materials, including Na_2CeF_6 (3.89 eV),[26] $CeF_2(SO_4)$ (2.71 eV), $Ce(IO_3)_2(SO_4)$ (2.42 eV), $CeF_2(IO_3)_2$ (2.17 eV), $Ce(IO_3)_2F_2{\cdot}H_2O$ (2.60 eV), $Ce_3F_4(SO_4)_4$ (2.5 eV), $Ba_2Ce(IO_3)_8(H_2O)$ (2.44 eV), and $Rb_2Ce(IO_3)_5F$ (2.35 eV).[59–65]

Thermal properties

The TG–DTA curves of $NH_4Ce_3F_{13}$ are presented in Fig. 5. From the curves, we can observe that $NH_4Ce_3F_{13}$ can be stable at temperatures below about 260 °C.

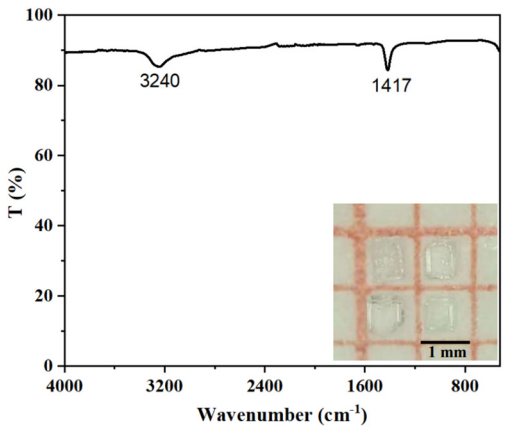

Fig. 3 IR spectrum of $NH_4Ce_3F_{13}$.

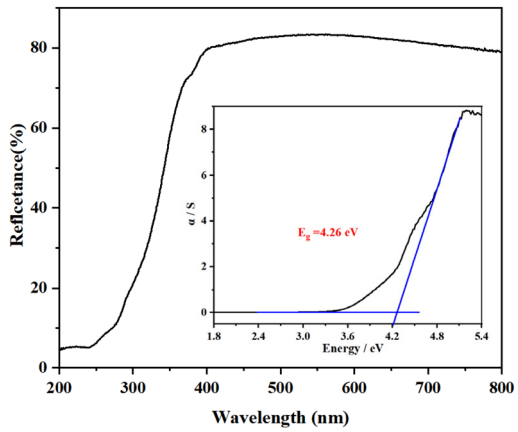

Fig. 4 UV–vis–NIR diffuse reflectance spectrum of $NH_4Ce_3F_{13}$. Inset: band gap of $NH_4Ce_3F_{13}$.

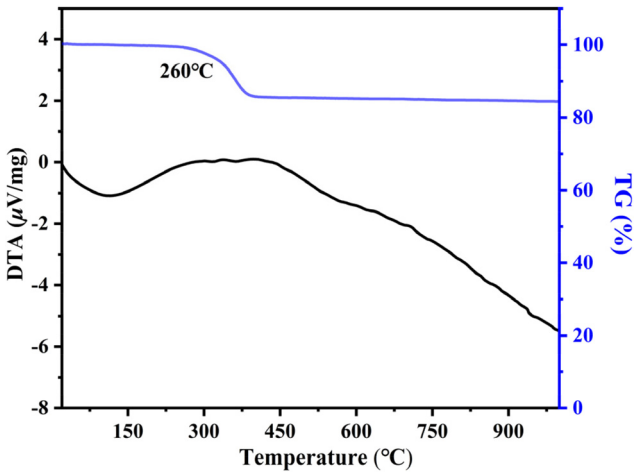

Fig. 5 TG–DTA curves of $NH_4Ce_3F_{13}$.

SHG activity and LIDT

Due to the acentric structure of $NH_4Ce_3F_{13}$, its SHG measurement was performed using the Kurtz–Perry method under a 1064 nm laser. The result shows that $NH_4Ce_3F_{13}$ exhibits an SHG efficiency of about 1.2 times that of KDP and can achieve phase-matching (Fig. 6), which is larger than most of the NLO fluoride crystals, including $BaZnF_4$ (0.16 × KDP), KBi_4F_{13} (0.5 × KDP), $SrAlF_5$ (0.65 × KDP), KNa_2ZrF_7 (0.4 × KDP), $K_3Ba_2Zr_6F_{31}$ (0.5 × KDP),[19–23] $CsNaTaF_7$ (0.2 × KDP),[27] and Na_2SbF_5 (0.17 × KDP).[66] Since $NH_4Ce_3F_{13}$ exhibits a large band gap and good SHG effect, the LIDTs of $NH_4Ce_3F_{13}$ and $AgGaS_2$ were measured under the same conditions. The LIDT measurement results show that $NH_4Ce_3F_{13}$ possesses a large LIDT value of 169.4 MW cm^{-2}, which is 39 times that of AGS (4.3 MW cm^{-2}). The LIDT value of $NH_4Ce_3F_{13}$ is much enhanced compared to other NLO halides (Table S8†), such as Na_2CeF_6 (20 × AGS), $Pb_7F_{12}Cl_2$ (15.4 × AGS), and KBi_4F_{13} (24 × AGS). Although the SHG signal is not stronger than Na_2CeF_6 (2.1 × KDP), $NH_4Ce_3F_{13}$ shows a larger band gap and higher LIDT than

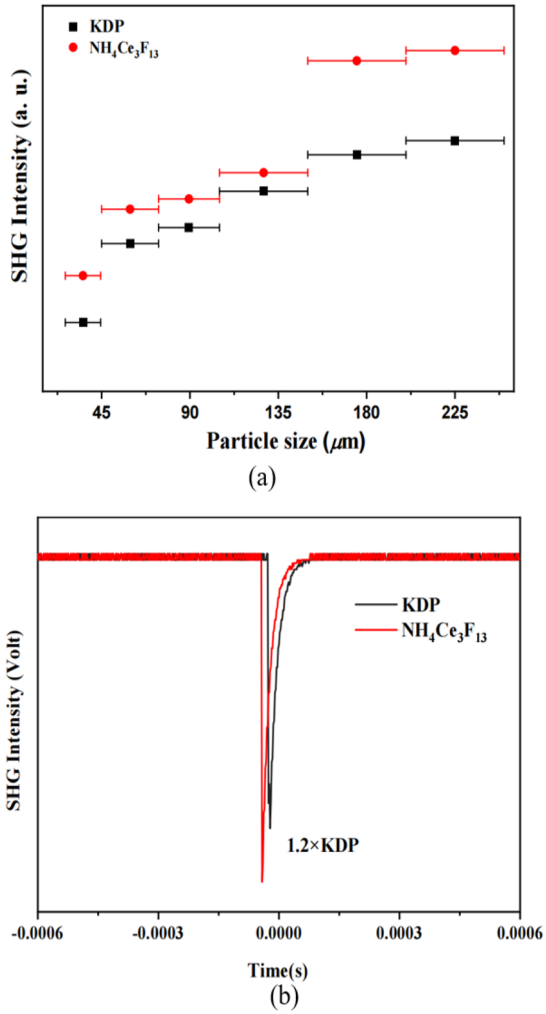

Fig. 6 (a) Size-dependence SHG responses of $NH_4Ce_3F_{13}$ and KDP under 1064 nm radiation, and (b) SHG responses of 200–250 μm particles of $NH_4Ce_3F_{13}$ and KDP.

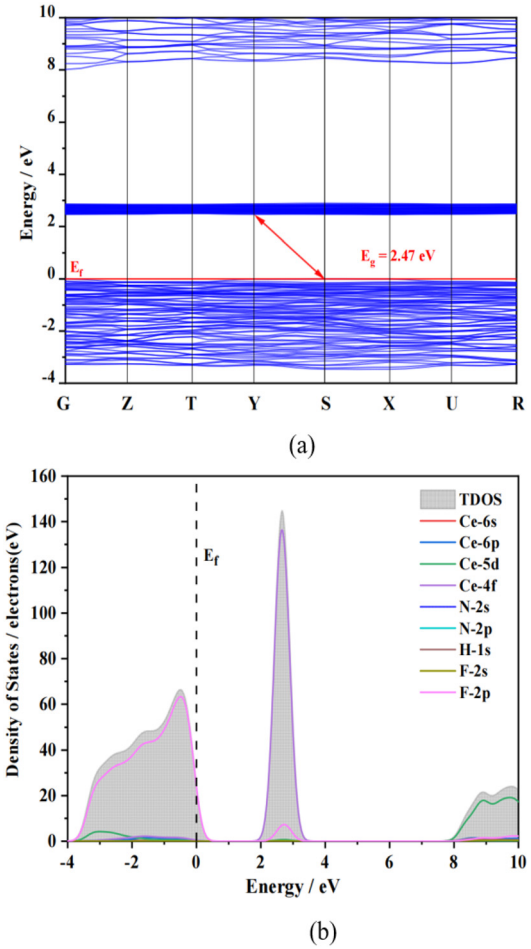

Fig. 7 Calculated (a) band gap and (b) density of states (DOS) of $NH_4Ce_3F_{13}$. The Fermi level is set at 0 eV.

Na_2CeF_6. Hence, $NH_4Ce_3F_{13}$ exhibits balanced NLO performance.

Theoretical studies

Based on the first principles calculations, we further study the relationship between structures and optical performances.[67] The calculated results indicate that the theoretical band gap of $NH_4Ce_3F_{13}$ is 2.47 eV (Fig. 7a). Due to the derivative discontinuity of the exchange–correlation function of GGA-PBE, the calculated band gap is smaller than the measured band gap. From the partial density of state (PDOS) graphs of $NH_4Ce_3F_{13}$ shown in Fig. 7b, the top of the valence band is mainly contributed by the F-2p orbitals. The bottom of the conduction band is mainly composed of Ce-4f and partial F-2p orbitals. Therefore, it can be observed that the charge transfer between the valence and conduction bands is mainly determined by the Ce and F atoms.

We deeply explore the NLO properties of $NH_4Ce_3F_{13}$ by calculation. As crystallized in the *mm*2 point group and considered Kleinman symmetry, $NH_4Ce_3F_{13}$ has three independent SHG tensors (χ_{31}, χ_{32}, and χ_{33}), which are calculated to be 0.50, 0.53, and 0.57 pm V^{-1} under a 1064 nm laser, respectively (Fig. 8a). The largest value is 0.7 times that of the KDP (d_{36} = 0.39 pm V^{-1}), which is relatively smaller than the experimental value. The underestimation is a deviation between the experiment and calculation, and similar cases have been reported in other works.[68,69] As the calculated refractive index dispersion curves of $NH_4Ce_3F_{13}$ shown in Fig. 8b, the calculated birefringence is 0.03@1064 nm, which is suitable for the phase-matching requirement. The phase-matching wavelength condition was also calculated (Fig. 8c), indicating that the shortest SHG phase-matching wavelength of $NH_4Ce_3F_{13}$ is 685 nm, which confirms the experimental results.

To further study the contribution of the groups in $NH_4Ce_3F_{13}$ to optical properties, the calculation of the electronic density difference is carried out. As presented in Fig. 9, the electron density of the F^- anion connected by the Ce^{4+} cation is higher. Therefore, the electron density difference map confirms that the CeF_9 polyhedra in $NH_4Ce_3F_{13}$ are the main contributors to NLO performance. Besides, the degree of distortion of the total CeF_9 polyhedra is also calculated, as

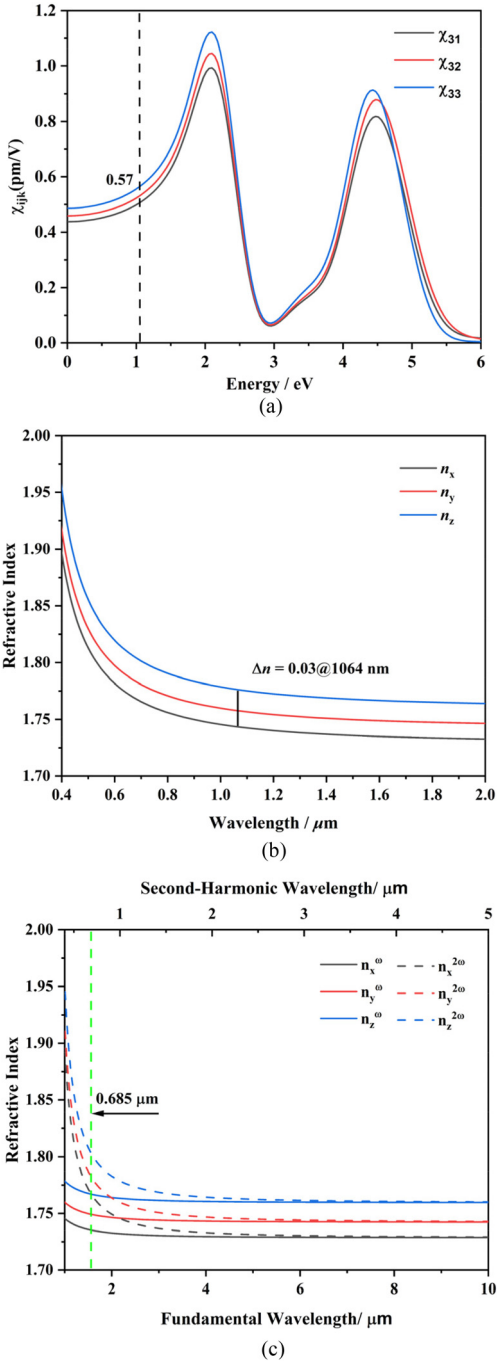

Fig. 8 Energy-dependent SHG tensors (a), calculated refractive index dispersion curves (b), and phase-matching conditions of $NH_4Ce_3F_{13}$ (c).

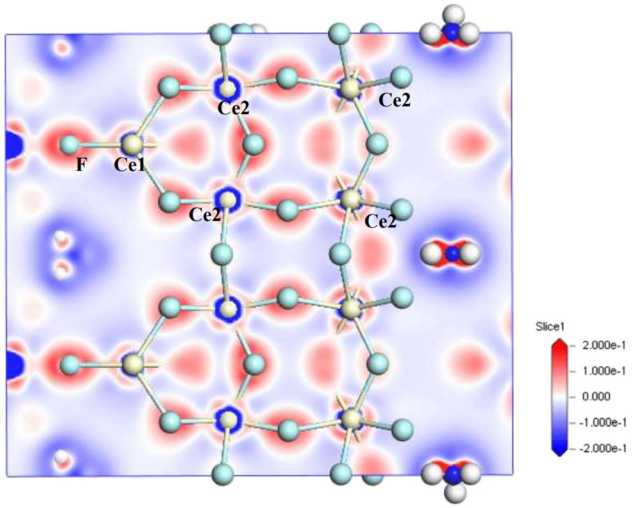

Fig. 9 Electron-density difference map of $NH_4Ce_3F_{13}$.

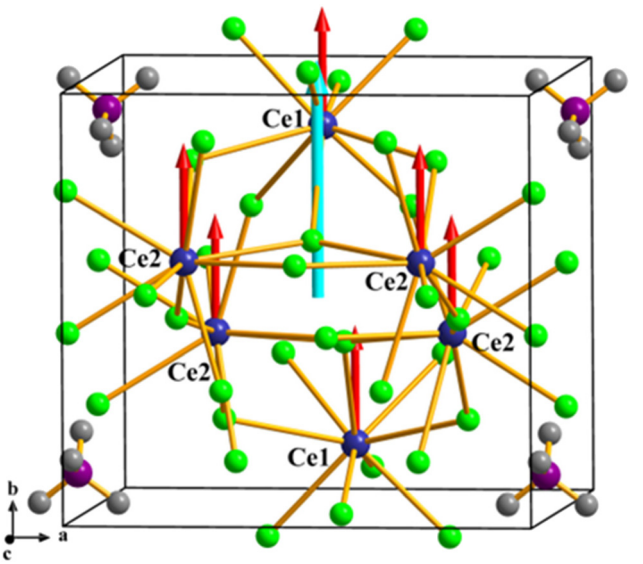

Fig. 10 Calculated dipole moments of $NH_4Ce_3F_{13}$ (red: CeF_9, blue: total).

shown in Table S9.† The calculation results reveal that CeF_9 polyhedra have a relatively large degree of distortion, which is beneficial for NLO properties. The dipole moments of two types of CeF_9 units and the total structure in one unit cell of $NH_4Ce_3F_{13}$ were calculated to analyse the contribution to the NLO effects. The results are shown in Fig. 10 and Table S10,† indicating that the dipole moments of CeF_9 units are arranged in almost the same orientation ranging from 0.55 to 1.10 D and the total dipole moment of CeF_9 units is 2.40 D, which results in SHG performance for $NH_4Ce_3F_{13}$. Obviously, the optical properties of $NH_4Ce_3F_{13}$ are determined by CeF_9 units.

Conclusions

In conclusion, $NH_4Ce_3F_{13}$, a Ce(IV)-based fluoride NLO crystal, was synthesized using a hydrothermal reaction. It displays a three-dimensional framework comprising corner- and edge-shared CeF_9 polyhedra. $NH_4Ce_3F_{13}$ exhibits a strong SHG response and high LIDT. Besides, $NH_4Ce_3F_{13}$ possesses the largest band gap among all the reported Ce(IV)-based NLO

materials. This study provides a good route to explore Ce(IV) halides with NLO effects. We will continue to develop more new promising NLO rare earth halide compounds.

Data availability

The data supporting the research findings of this work are available from the corresponding author on reasonable request.

Conflicts of interest

The authors declare that they have no conflict of interest.

Acknowledgements

The authors acknowledge financial support from the National Natural Science Foundation of China (22101248), the Lvyangjinfeng Talent Program of Yangzhou (YZLYJFJH2021YXBS083), and the Qinglan Project of Yangzhou University.

References

1 P. F. Gong, F. Liang, L. Kang, X. G. Chen, J. G. Qin, Y. C. Wu and Z. S. Lin, Recent advances and future perspectives on infrared nonlinear optical metal halides, *Coord. Chem. Rev.*, 2019, **380**, 83–102.

2 Y. Pan, S. P. Guo, B. W. Liu, H. G. Xue and G. C. Guo, Second-order nonlinear optical crystals with mixed anions, *Coord. Chem. Rev.*, 2018, **374**, 464–496.

3 H. Cho, S. H. Jeong, M. H. Park, Y. H. Kim, C. Wolf, C. L. Lee, J. H. Heo and A. Sadhanala, Overcoming the electroluminescence efficiency limitations of perovskite light-emitting diodes, *Science*, 2015, **350**, 1222–1225.

4 F. G. You, F. Liang, Q. Huang, Z. G. Hu, Y. C. Wu and Z. S. Lin, $Pb_2GaF_2(SeO_3)_2Cl$: Band Engineering Strategy by Aliovalent Substitution for Enlarging Bandgap while Keeping Strong Second Harmonic Generation Response, *J. Am. Chem. Soc.*, 2019, **141**, 748–752.

5 Y. Huang, X. G. Meng, P. F. Gong, Z. S. Lin, X. G. Chen and J. G. Qin, A Study on $K_2SbF_2Cl_3$ as A New Mid-IR Nonlinear Optical Material: New Synthesis and Excellent Properties, *J. Mater. Chem. C*, 2015, **3**, 9588–9593.

6 Q. Wu, X. Liu, F. Liang, S. R. Xu, H. B. Pi, X. Han, Y. Liu, Z. S. Lin and Y. J. Li, $Pb_7F_{12}Cl_2$: A Promising Infrared Nonlinear Optical Material with High Laser Damage Threshold, *Dalton Trans.*, 2019, **48**, 13529–13535.

7 M. Zhang, S. L. Pan, Z. H. Yang, Y. Wang, X. Su, Y. Yang, Z. J. Huang, S. J. Han and K. R. Poeppelmeier, $BaClBF_4$: a new noncentrosymmetric pseudo-Aurivillius type material with transparency range from deep UV to middle IR and a high laser damage threshold, *J. Mater. Chem. C*, 2013, **1**, 4740–4745.

8 C. Yang, X. Liu, C. Teng, X. Cheng, F. Liang and Q. Wu, Hierarchical molecular design of high-performance infrared nonlinear Ag_2HgI_4 material by defect engineering strategy, *Mater. Today Phys.*, 2021, **19**, 100432.

9 Q. Wu, C. Yang, J. Ma, X. Liu and Y. J. Li, Halogen-Ion-Induced Structural Phase Transition Giving a Polymorph of $HgBr_2$ with Balanced Nonlinear Optical Properties, *Inorg. Chem.*, 2021, **60**, 19297–19303.

10 S. W. Lv, Q. Wu, X. G. Meng, L. Kang, C. Zhong, Z. S. Lin, Z. G. Hu, X. G. Chen and J. G. Qin, A promising new nonlinear optical crystal with high laser damage threshold for application in the IR region: synthesis, crystal structure and properties of noncentrosymmetric $CsHgBr_3$, *J. Mater. Chem. C*, 2014, **2**, 6796–6801.

11 G. Zhang, Y. J. Li, K. Jiang, H. Y. Zeng, T. Liu, X. G. Chen, J. G. Qin, Z. S. Lin, P. Z. Fu, Y. C. Wu and C. T. Chen, A New Mixed Halide, $Cs_2HgI_2Cl_2$: Molecular Engineering for a New Nonlinear Optical Material in the Infrared Region, *J. Am. Chem. Soc.*, 2012, **134**, 14818–14822.

12 Q. Wu, X. G. Meng, C. Zhong, X. G. Chen and J. G. Qin, $Rb_2CdBr_2I_2$: A New IR Nonlinear Optical Material with a Large Laser Damage Threshold, *J. Am. Chem. Soc.*, 2014, **136**, 5683–5686.

13 Q. Wu, X. Liu, Y. S. Du, C. L. Teng and F. Liang, Abnormal bandgap enlargement resulted in a promising mid-infrared nonlinear optical material Rb_2CdBrI_3 with an ultrahigh laser damage threshold, *J. Mater. Chem. C*, 2020, **8**, 9005–9011.

14 P. F. Gong, S. Y. Luo, Y. Yang, F. Liang, S. Z. Zhang, S. G. Zhao, J. H. Luo and Z. S. Lin, Nonlinear Optical Crystal $Rb_4Sn_3Cl_2Br_8$: Synthesis, Structure, and Characterization, *Cryst. Growth Des.*, 2017, **18**, 380–385.

15 J. Y. Guo, J. B. Huang, A. Tudi, X. L. Hou, S. J. Han, Z. H. Yang and S. L. Pan, Birefringence Regulation by Clarifying the Relationship Between Stereochemically Active Lone Pairs and Optical Anisotropy in Tin-based Ternary Halides, *Angew. Chem., Int. Ed.*, 2023, **62**, e202304238.

16 J. B. Wang, M. M. Zhu, Y. Q. Chu, J. D. Tian, L. L. Liu, B. B. Zhang and P. S. Halasyamani, Rational Design of the Alkali Metal Sn-Based Mixed Halides with Large Birefringence and Wide Transparent Range, *Small*, 2024, **20**, 2308884.

17 G. Zhang, T. Liu, T. X. Zhu, J. G. Qin, Y. C. Wu and C. T. Chen, SbF_3: A new second-order nonlinear optical material, *Opt. Mater.*, 2008, **31**, 110–113.

18 G. Zhang, J. G. Qin, T. Liu, Y. J. Li, Y. C. Wu and C. T. Chen, $NaSb_3F_{10}$: A new second-order nonlinear optical crystal to be used in the IR region with very high laser damage threshold, *Appl. Phys. Lett.*, 2009, **95**, 261104.

19 J. G. Bergman, G. R. Crane and H. Guggenheim, Linear and nonlinear optical properties of ferroelectric $BaMgF_4$ and $BaZnF_4$, *J. Appl. Phys.*, 1975, **46**, 4645.

20 Q. Wu, H. M. Liu, F. C. Jinang, X. G. Meng, X. G. Chen, L. Yang, Z. G. Hu and J. G. Qin, KBi_4F_{13}: An Infrared

Nonlinear Optical Material with High Laser Damage Threshold, *Inorg. Chem.*, 2015, **31**, 1875–1880.

21 H. Huang, Z. S. Lin, L. Bai, R. He and C. T. Chen, Mechanism of the linear and nonlinear optical effects of $SrAlF_5$ and $BaMgF_4$ crystals, *Solid State Commun.*, 2010, **150**, 2318–2321.

22 X. Lian, W. D. Yao, W. L. Liu, R. L. Tang and S. P. Guo, KNa_2ZrF_7: A Mixed-Metal Fluoride Exhibits Phase-Matchable Second-Harmonic-Generation Effect and High Laser-Induced Damage Threshold, *Inorg. Chem.*, 2021, **60**, 19–23.

23 M. Yan, R. L. Tang, W. D. Yao, W. L. Liu and S. P. Guo, Exploring a new short-wavelength nonlinear optical fluoride material featuring unprecedented polar cis-$[Zr_6F_{34}]^{10-}$ clusters, *Chem. Sci.*, 2024, **15**, 2883–2888.

24 M. Yan, R. L. Tang, W. D. Yao, W. L. Liu and S. P. Guo, From $CaBaM_2F_{12}$ to $K_2BaM_2F_{12}$ (M = Zr, Hf): Heterovalent Cation-Substitution-Induced Symmetry Break and Nonlinear-Optical Activity, *Inorg. Chem.*, 2024, **63**, 10949–10953.

25 M. Yan, R. L. Tang, W. Xu, W. L. Liu and S. P. Guo, Centrosymmetric $CaBaMF_8$ and Noncentrosymmetric Li_2CaMF_8 (M = Zr, Hf): Dimension Variation and Nonlinear Optical Activity Resulting from an Isovalent Cation Substitution-Oriented Design, *Inorg. Chem.*, 2024, **63**, 5260–5268.

26 R. L. Tang, W. Xu, X. Lian, Y. Q. Wei, Y. L. Lv, W. L. Liu and S. P. Guo, Na_2CeF_6: A Highly Laser Damage-Tolerant Double Perovskite Type Ce(IV) Fluoride Exhibiting Strong Second-Harmonic-Generation Effect, *Small*, 2024, **20**, 2308348.

27 R. L. Tang, X. Lian, X. H. Li, L. Huai, W. L. Liu and S. P. Guo, From $CsKTaF_7$ to $CsNaTaF_7$: Alkali Metal Cations Regulation to Generate SHG Activity, *Chem. – Eur. J.*, 2022, **28**, e202201588.

28 Z. F. Song, H. W. Yu, H. P. Wu, Z. G. Hu, J. Y. Wang and Y. C. Wu, Syntheses, structures and characterization of non-centrosymmetric $Rb_2Zn_3(P_2O_7)_2$ and centrosymmetric $Cs_2M_3(P_2O_7)_2$ (M = Zn and Mg), *Inorg. Chem. Front.*, 2020, **7**, 3482–3490.

29 Y. Zheng, Z. J. Wei, H. P. Wu, Z. G. Hu, J. Y. Wang, Y. C. Wu and H. W. Yu, Breaking through the "200 nm deep-ultraviolet wall" of phase matching region by cation structural modulation, *Mater. Today Phys.*, 2024, **46**, 101529.

30 H. P. Wu, Z. J. Wei, Z. G. Hu, J. Y. Wang, Y. C. Wu and H. W. Yu, Assembly of π-Conjugated $[B_3O_6]$ Units by Mer-Isomer $[YO_3F_3]$ Octahedra to Design a UV Nonlinear Optical Material, $Cs_2YB_3O_6F_2$, *Angew. Chem., Int. Ed.*, 2024, **63**, e202406318.

31 X. M. He, L. Qi, W. Y. Zhang, R. X. Zhang, X. Y. Dong, J. H. Ma, M. Abudoureheman, Q. Jing and Z. H. Chen, Controlling the Nonlinear Optical Behavior and Structural Transformation with A-Site Cation in α-$AZnPO_4$ (A = Li, K), *Small*, 2023, **19**, 2206991.

32 Z. Z. Zhang, Y. Wang, B. B. Zhang, Z. H. Yang and S. L. Pan, Polar Fluorooxoborate, NaB_4O_6F: A Promising Material for Ionic Conduction and Nonlinear Optics, *Angew. Chem., Int. Ed.*, 2018, **57**, 6577–6581.

33 G. Q. Shi, Y. Wang, F. F. Zhang, B. B. Zhang, Z. H. Yang, X. L. Hou, S. L. Pan and K. R. Poeppelmeier, Finding the Next Deep-Ultraviolet Nonlinear Optical Material: $NH_4B_4O_6F$, *J. Am. Chem. Soc.*, 2017, **139**, 10645–10648.

34 F. Liang, L. Kang, P. F. Gong, Z. S. Lin and Y. C. Wu, Rational Design of Deep-Ultraviolet Nonlinear Optical Materials in Fluorooxoborates: Toward Optimal Planar Configuration, *Chem. Mater.*, 2017, **29**, 7098–7102.

35 X. F. Wang, Y. Wang, B. B. Zhang, F. F. Zhang, Z. H. Yang and S. L. Pan, CsB_4O_6F: A Congruent-Melting Deep-Ultraviolet Nonlinear Optical Material by Combining Superior Functional Units, *Angew. Chem., Int. Ed.*, 2017, **56**, 14119–14123.

36 Y. Wang, B. B. Zhang, Z. H. Yang and S. L. Pan, Cation-Tuned Synthesis of Fluorooxoborates: Towards Optimal Deep-Ultraviolet Nonlinear Optical Materials, *Angew. Chem., Int. Ed.*, 2018, **57**, 2150–2154.

37 G. h. Zou, N. Ye, L. Huang and X. S. Lin, Alkaline-Alkaline Earth Fluoride Carbonate Crystals $ABCO_3F$ (A = K, Rb, Cs; B = Ca, Sr, Ba) as Nonlinear Optical Materials, *J. Am. Chem. Soc.*, 2011, **133**, 20001–20007.

38 Z. Q. Xie, M. Mutailipu, G. J. He, G. P. Han, Y. Wang, Z. H. Yang, M. Zhang and S. L. Pan, A Series of Rare-Earth Borates $K_7MRE_2B_{15}O_{30}$ (M = Zn, Cd, Pb; RE = Sc, Y, Gd, Lu) with Large Second Harmonic Generation Responses, *Chem. Mater.*, 2018, **30**, 2414–2423.

39 V. Dolomanov, L. J. Bourhis, R. J. Gildea, J. A. K. Howard and H. Puschmann, OLEX2: A complete structure solution, refinement and analysis program, *J. Appl. Crystallogr.*, 2009, **42**, 339–341.

40 J. Tauc, R. Grigorovici and A. Vancu, Optical Properties and Electronic Structure of Amorphous Germanium, *Phys. Status Solidi B*, 1966, **15**, 627–637.

41 S. K. Kurtz and T. T. Perry, A Powder Technique for the Evaluation of Nonlinear Optical Materials, *J. Appl. Phys.*, 1968, **39**, 3798–3813.

42 S. J. Clark, M. D. Segall, C. J. Pickard, P. J. Hasnip, M. J. Probert, K. Refson and M. C. Z. Payne, First Principles Methods Using CASTEP, *Z. Kristallogr. - Cryst. Mater.*, 2005, **220**, 567–570.

43 D. D. Macdonald and M. Urquidi-Macdonald, Application of Kramers-Kronig Transforms in the Analysis of Electrochemical Systems: I. Polarization Resistance, *J. Electrochem. Soc.*, 1985, **132**, 2316–2319.

44 A. Grzechnik, C. C. Underwood, J. W. Kolis and K. Friese, Crystal structures and stability of $LiCeF_5$ and $LiThF_5$ at high pressures: A comparative study of the coordination around the Ce^{4+} and Th^{4+} ions, *J. Fluor. Chem.*, 2013, **156**, 124–129.

45 R. Hoppe and K. M. Roedder, Fluorokomplexe des vierwertigen Cers, *Z. Anorg. Allg. Chem.*, 1961, **313**, 154–160.

46 A. Grzechnik, C. C. Underwood and J. W. Kolis, Twinned caesium cerium(IV) pentafluoride, *Acta Crystallogr., Sect. B: Struct. Sci.*, 2014, **70**, 112–113.

47 C. J. Windorff, A. T. Chemey, J. M. Sperling, B. E. Klamm and T. E. Albrecht-Schmitt, Examination of Molten Salt Reactor Relevant Elements Using Hydrothermal Synthesis, *Inorg. Chem.*, 2020, **59**, 4176–4180.

48 C. C. Underwood, C. D. Mcmillen and J. W. Kolis, Hydrothermal Synthesis and Crystal Chemistry of Novel Fluorides with $A_7B_6F_{31}$ (A = Na, K, NH_4, Tl; B = Ce, Th) Compositions, *J. Chem. Crystallogr.*, 2014, **44**, 493–500.

49 R. R. Ryan, A. C. Larson and F. H. Kruse, Crystal Structure of Ammonium Hexafluorocerate(IV), $(NH_4)_2CeF_6$, *Inorg. Chem.*, 1969, **8**, 33–36.

50 S. J. Patwe, B. N. Wani, U. R. K. Rao and K. S. Venkateswarlu, Synthesis and thermal study of tris (ammonium) hexafluoro metallates(III) of some rare earths, *Can. J. Chem.*, 1989, **67**, 1815–1818.

51 L. A. Zemnukhova, A. A. Udovenko, N. V. Makarenko, S. I. Kuznetsov and T. A. Babushkina, Crystal structure and Sb NQR Parameters of ammonium tridecafluorotetraantimonate(III) $NH_4Sb_4F_{13}$, *J. Struct. Chem.*, 2017, **58**, 694–699.

52 A. A. Udovenko, L. A. Zemnukhova, Y. E. Gorbunova, Y. N. Mikhailov and R. L. Davidovich, Crystal Structure of Thallium Tridecafluorotetraantimonate(III) $TlSb_4F_{13}$, *Russ. J. Coord. Chem.*, 2003, **29**, 310–311.

53 J. Yeon, M. D. Smith, J. Tapp, A. Möller and H. C. zur Loye, Mild Hydrothermal Crystal Growth, Structure, and Magnetic Properties of Ternary U(IV) Containing Fluorides: $LiUF_5$, KU_2F_9, $K_7U_6F_{31}$, $RbUF_5$, RbU_2F_9, and RbU_3F_{13}, *Inorg. Chem.*, 2014, **53**, 6289–6298.

54 H. Abazli, A. Cousson, A. Tabuteau and M. Pages, Fluorure d'Ammonium et d'Uranium(IV): $NH_4U_3F_{13}$, *Acta Crystallogr., Sect. B: Struct. Crystallogr. Cryst. Chem.*, 1980, **36**, 2765–2766.

55 C. C. Underwood, M. Mann, C. D. McMillen and J. W. Kolis, Hydrothermal Descriptive Chemistry and Single Crystal Structure Determination of Cesium and Rubidium Thorium Fluorides, *Inorg. Chem.*, 2011, **50**, 11825–11831.

56 J. H. Wu, C. L. Hu, Y. F. Li, J. G. Mao and F. Kong, $[(C_5H_6N_2)_2H](Sb_4F_{13})$: a polyfluoroantimonite with a strong second harmonic generation effect, *Chem. Sci.*, 2024, **15**, 8071–8079.

57 Q. Wang, J. X. Ren, D. Wang, L. L. Cao, X. H. Dong, L. Huang, D. J. Gao and G. H. Zou, Low temperature molten salt synthesis of noncentrosymmetric $(NH_4)_3SbF_3(NO_3)_3$ and centrosymmetric $(NH_4)_3SbF_4(NO_3)_2$, *Inorg. Chem. Front.*, 2023, **10**, 2107–2114.

58 Q. Wu, C. Yang, X. Liu, J. Ma, F. Liang and Y. S. Du, Dimensionality reduction made high-performance mid-infrared nonlinear halide crystal, *Mater. Today Phys.*, 2021, **21**, 100569.

59 C. Wu, T. H. Wu, X. X. Jiang, Z. J. Wang, H. Y. Sha, L. Lin, Z. S. Lin, Z. P. Huang, X. F. Long, M. G. Humphrey and C. Zhang, Large Second-Harmonic Response and Giant Birefringence of $CeF_2(SO_4)$ Induced by Highly Polarizable Polyhedra, *J. Am. Chem. Soc.*, 2021, **143**, 4138–4142.

60 T. H. Wu, X. X. Jiang, Y. R. Zhang, Z. J. Wang, H. Y. Sha, C. Wu, Z. S. Lin, Z. P. Huang, X. F. Long, M. G. Humphrey and C. Zhang, From $CeF_2(SO_4)\cdot H_2O$ to $Ce(IO_3)_2(SO_4)$: Defluorinated Homovalent Substitution for Strong Second-Harmonic-Generation Effect and Sufficient Birefringence, *Chem. Mater.*, 2021, **33**, 9317–9325.

61 T. H. Wu, X. X. Jiang, C. Wu, H. Y. Sha, Z. J. Wang, Z. S. Lin, Z. P. Huang, X. F. Long, M. G. Humphrey and C. Zhang, From $Ce(IO_3)_4$ to $CeF_2(IO_3)_2$: fluorinated homovalent substitution simultaneously enhances SHG response and bandgap for mid-infrared nonlinear optics, *J. Mater. Chem. C*, 2021, **9**, 8987–8993.

62 T. Abudouwufu, M. Zhang, S. C. Cheng, Z. H. Yang and S. L. Pan, $Ce(IO_3)_2F_2\cdot H_2O$: The First Rare-Earth-Metal Iodate Fluoride with Large Second Harmonic Generation Response, *Chem. – Eur. J.*, 2019, **25**, 1221–1226.

63 T. H. Wu, X. X. Jiang, C. Wu, Z. S. Lin, Z. P. Huang, M. G. Humphrey and C. Zhang, $Ce_3F_4(SO_4)_4$: cationic framework assembly for designing polar nonlinear optical material through fluorination degree modulation, *Inorg. Chem. Front.*, 2023, **10**, 5270–5277.

64 X. Y. Zhang, X. H. Zhang, B. P. Yang and J. G. Mao, A new polar alkaline earth–rare earth iodate: $Ba_2Ce(IO_3)_8(H_2O)$, *Dalton Trans.*, 2023, **52**, 4423–4428.

65 O. P. Grigorieva, T. B. Shatalova, A. N. Kuznetsov, P. S. Berdonosov, S. Yu. Stefanovich, K. A. Lyssenko and V. A. Dolgikh, New iodate fluoride $Rb_2Ce(IO_3)_5F$ with nonlinear optical properties, *Dalton Trans.*, 2024, **53**, 7367–7375.

66 J. G. Bergman, D. S. Chemla, R. Fourcade and G. Mascherpa, Linear and nonlinear optical properties of Na_2SbF_5, *J. Solid State Chem.*, 1978, **23**, 187–190.

67 J. P. Perdew and M. Levy, Physical Content of the Exact Kohn-Sham Orbital Energies: Band Gaps and Derivative Discontinuities, *Phys. Rev. Lett.*, 1983, **51**, 1884–1887.

68 Y. Q. Wei, W. Xu, L. Huai, Y. L. Lv, W. L. Liu, S. P. Guo and R. L. Tang, From ZnF_2 to $ZnF_2(H_2O)_4$: Partial Substitution Achieves Structural Transformation and Nonlinear Optical Activity while Keeping Short Ultraviolet Cutoff Edge, *Inorg. Chem.*, 2024, **63**, 1714–1719.

69 M. Yan, C. L. Hu, R. L. Tang, W. D. Yao, W. L. Liu and S. P. Guo, $KBa_3M_2F_{14}Cl$ (M = Zr, Hf): novel short-wavelength mixed metal halides with the largest second-harmonic generation responses contributed by mixed functional moieties, *Chem. Sci.*, 2024, **15**, 8500–8505.

